

Age of the Cenomanian–Turonian boundary in the Western Interior of the United States

*Bart J. Kowallis, *Eric H. Christiansen, †Alan L. Deino,
‡Michael J. Kunk and §Larry M. Heaman

*Department of Geology, Brigham Young University, Provo, UT 84602, USA

† Geochronology Center, Institute of Human Origins, 2453 Ridge Road, Berkeley, CA 94709, USA

‡ U.S. Geological Survey, 981 National Center, Reston, VA 22092, USA

§ Department of Geology, Royal Ontario Museum, Toronto, Ontario, Canada M5S 2C6

Received 5 February 1993 and accepted 28 October 1994

High precision $^{40}\text{Ar}/^{39}\text{Ar}$ laser-microprobe ages of individual sanidines, $^{40}\text{Ar}/^{39}\text{Ar}$ plateau age spectra on bulk sanidine concentrates, U-Pb zircon ages, and zircon and apatite fission-track ages from three bentonites bracketing the Cenomanian-Turonian boundary in the Western Interior of the United States suggest an age for the boundary of 93.1 ± 0.3 (2σ). The lowermost bentonite comes from the Upper Cenomanian *Sciponoceras gracile* biozone, and gives a weighted mean laser-fusion single-crystal $^{40}\text{Ar}/^{39}\text{Ar}$ age of 93.50 ± 0.52 Ma (2σ , standard error of the mean, $n = 14$) for sanidine. The middle bentonite comes from the Upper Cenomanian *Neocardioceras juddii* biozone, accepted in both North America and Europe as the uppermost Cenomanian ammonite zone; it gives an average single-crystal $^{40}\text{Ar}/^{39}\text{Ar}$ age of 93.33 ± 0.50 Ma ($n = 29$), a bulk-sample $^{40}\text{Ar}/^{39}\text{Ar}$ plateau age of 93.09 ± 0.34 Ma (2σ) for sanidine, and concordant $^{206}\text{Pb}/^{238}\text{U}$ and $^{207}\text{Pb}/^{235}\text{U}$ ages of 93.48 ± 0.32 Ma on zircon. The upper bentonite comes from near the base of the Turonian, immediately above the first occurrence of the basal Turonian bivalve *Mytiloides* and sanidines from it give an average single-crystal $^{40}\text{Ar}/^{39}\text{Ar}$ age of 93.46 ± 0.60 Ma ($n = 12$) and a bulk-sample $^{40}\text{Ar}/^{39}\text{Ar}$ plateau age of 92.87 ± 0.34 Ma. The composition of these Cenomanian–Turonian bentonites from Colorado and Utah, the types of phenocrysts present, and the morphology of included zircons all indicate that the pre-alteration ash was rhyolitic and probably generated in a subduction setting involving a significant crustal component.

KEY WORDS: $^{40}\text{Ar}/^{39}\text{Ar}$ ages; Cenomanian; Turonian; geologic time scale; Western Interior; USA.

1. Introduction

Time scales are frequently revised as new techniques allow us to determine the apparent ages of mineral grains in rocks more precisely. With the recent interest in causes and timing of mass extinction events, it is increasingly important to have precise age information for all portions of the geologic time scale, and in particular for those which involved significant extinctions like the one at the Cenomanian–Turonian boundary (Raupe & Sepkoski, 1982; Kauffman, 1984; Elder, 1987). Most age data, before now, have come from analyses of groups of grains, providing average ages of bulk crystal populations. Single-grain methods, such as fission track dating, have not been widely used because of large analytical errors associated with the ages of individual grains. The development of $^{40}\text{Ar}/^{39}\text{Ar}$ laser-fusion techniques, however, permits high-precision age determinations on single grains of suitable volcanic materials, principally sanidine. Although volcanic ash horizons are generally superb time markers, bentonites in sedimentary sections are often reworked and contaminated with older detrital grains, in addition to any contaminants the volcanic ash might have picked up during the eruption process. Single-grain ages provide a means of examining the

population of mineral ages within a sample, thus providing insight into the degree of contamination. In this study, we have combined the use of single-grain methods ($^{40}\text{Ar}/^{39}\text{Ar}$ laser-fusion and fission track) with high-precision multiple-grain methods ($^{40}\text{Ar}/^{39}\text{Ar}$ age spectrum and U–Pb) to provide a reliable geochronological calibration of the Cenomanian–Turonian boundary.

The age of the boundary has generally been placed at about 91 Ma (Obradovich & Cobban, 1975; Kennedy & Odin, 1982; Harland *et al.*, 1982, 1990; Palmer, 1983; Kent & Gradstein, 1986). Early Turonian K–Ar biotite ages from bentonites in the Seabee Formation (Alaska), however, have suggested that the boundary might be closer to 93 Ma (Lanphere & Tailleur, 1983). Figure 1 shows the distribution of late Cenomanian and early Turonian ages reported in Odin (1982), Lanphere & Tailleur (1983) and Elder (1988) (see also Table 1). Early Turonian ages range from about 89 Ma to 94 Ma, while late Cenomanian ages range from about 88 Ma to 97 Ma.

Preliminary single-crystal $^{40}\text{Ar}/^{39}\text{Ar}$ laser-fusion age results on Cenomanian–Turonian ash beds were obtained in 1989 (Kowallis *et al.*, 1989). These initial results suggested an older age for the boundary of about 94.5 Ma, but suffered from the fact that only a few sanidine grains were available for dating each sample. In addition, later examination of the data showed that reactor flux gradient effects had not been adequately taken into account. A larger number of grains were extracted from these localities and rerun with closer spatial monitoring of reactor flux. The new ages were reported in abstracts (Kowallis *et al.*, 1990, 1992) and are included in this paper. Obradovich (1991, 1992, 1994) has also been working on a revision of the Cenomanian–Turonian boundary. He proposes a boundary at 93.3 Ma. Shibata (1992) has also obtained ages ($92\text{--}95 \pm 2$ Ma) from tuffs in Cenomanian–Turonian sediments in Japan.

A key point, frequently ignored in time scale compilations, is that all ages are not of equal value. For example, Harland *et al.* (1982, 1990) and Odin (1982) continue to use glaucony ages in determining the age of Late Cretaceous stage boundaries even though glaucony has a systematic bias toward younger ages and, thus should be excluded (Obradovich, 1988). In order for an age to be useful in constraining the geologic time scale it must meet the following criteria:

- (1) The sample dated must record the time of deposition of the enclosing strata.
- (2) The isotopic system used in obtaining an age should be undisturbed by later thermal and alteration effects.
- (3) The sample must be well-constrained biostratigraphically; the position of the sample relative to key biostratigraphic boundaries should be known and generally accepted.
- (4) The degree of contamination of a sample from detrital and other sources should be known.
- (5) The isotopic dating system used should be of relatively high precision.

None of the samples listed in Table 1 meets all these criteria. The glaucony ages cannot record the time of deposition, because glauconite forms after deposition; the biotite ages come from samples low in potassium (<6%) and are therefore altered (except in the Alaskan samples) or have low precision; and none of the methods used can accurately detect contamination, alteration effects, or thermal disturbance of the samples. Our approach to dating the Cenomanian–Turonian boundary has been to try to satisfy all of the above criteria. Single-crystal $^{40}\text{Ar}/^{39}\text{Ar}$ laser-fusion ages provide a high-precision method that also gives

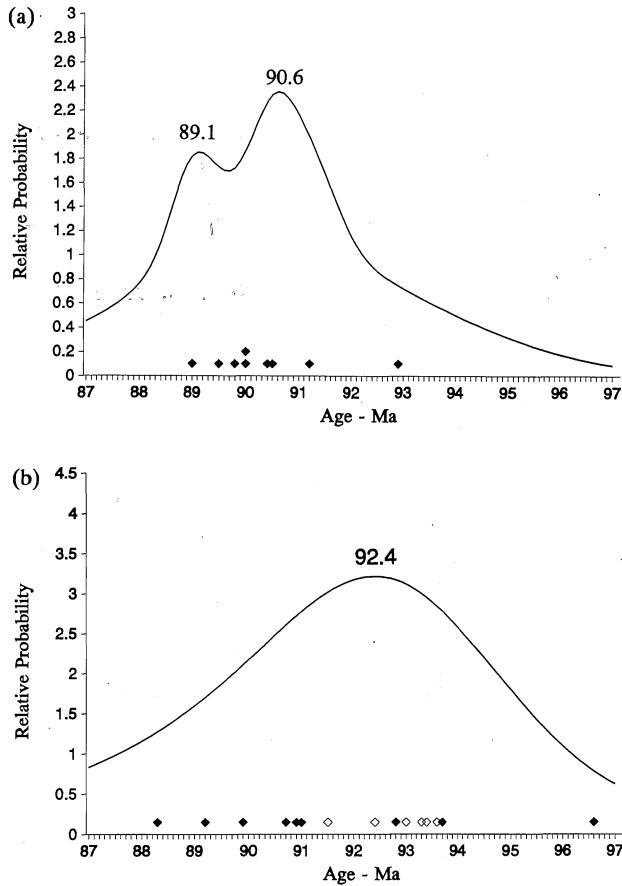


Figure 1. Probability plots for late Cenomanian-early Turonian ages from A, Europe and B, North America determined using the methods described in Hurford *et al.* (1984) and Kowallis *et al.* (1986). European ages are all glaucony ages and North American ages are K-Ar biotite and sanidine ages. The open diamonds on B represent early Turonian K-Ar ages from the Seabee Formation in Alaska. The North American plot gives a single age peak and a nearly bell-shaped curve while the European glaucony ages do not.

information on the degree of contamination of a sample; $^{40}\text{Ar}/^{39}\text{Ar}$ age-spectrum dating techniques provide high-precision ages as well as a measure of the basic assumption that the mineral phase represents a closed system to argon (no gain or loss of daughter isotope from the sample); fission track ages and apatite fission track length measurements provide information on the closure of the isotopic systems and the thermal history of the samples; and U-Pb dating of zircons provides an additional high-precision check on the age.

2. Stratigraphic setting

The samples dated were collected in 1987 on a Geological Society of America field excursion conducted by Kauffman *et al.* (1987). High resolution stratigraphic studies in the Bridge Creek Limestone, and equivalent formations to the west, have shown that ash beds near the Cenomanian-Turonian boundary can be located and correlated over wide areas of the Western Interior (Hattin, 1971, 1975, 1979, 1985; Elder, 1987, 1988). We collected samples of these ashes

Table 1. Late Cenomanian and early Turonian radiometric ages.

Location	Age \pm Error	Mineral	Method	Source
<i>early Turonian ages</i>				
Europe	89.0 \pm 0.4 Ma	Glaucony	K-Ar	Kreuzer <i>et al.</i> , 1982
Western Interior	89.2 \pm 3.3 Ma	Biotite	K-Ar	Elder, 1988
Western Interior	89.9 \pm 3.0 Ma	Biotite	K-Ar	Williams & Baadsgard, 1975
Europe	90.5 \pm 0.4 Ma	Glaucony	K-Ar	Kreuzer <i>et al.</i> , 1982
Western Interior	90.7 \pm 3.0 Ma	Sanidine	K-Ar	Williams & Baadsgard, 1975
Western Interior	90.9 \pm 3.4 Ma	Biotite	K-Ar	Elder, 1988
Western Interior	91.0 \pm 1.8 Ma	Biotite	K-Ar	Obradovich & Cobban, 1975
Alaska	91.5 \pm 0.9 Ma	Biotite	K-Ar	Lanphere & TAILLEUR, 1983
Alaska	92.4 \pm 0.9 Ma	Biotite	K-Ar	Lanphere & TAILLEUR, 1983
Alaska	93.0 \pm 0.9 Ma	Biotite	K-Ar	Lanphere & TAILLEUR, 1983
Alaska	93.3 \pm 0.9 Ma	Biotite	K-Ar	Lanphere & TAILLEUR, 1983
Alaska	93.4 \pm 1.3 Ma	Biotite	Ar-Ar	Lanphere & TAILLEUR, 1983
Alaska	93.6 \pm 1.2 Ma	Biotite	K-Ar	Lanphere & TAILLEUR, 1983
<i>late Cenomanian ages</i>				
Western Interior	72.5 \pm 2.5 Ma	Biotite	K-Ar	Elder, 1988
Western Interior	88.3 \pm 3.3 Ma	Biotite	K-Ar	Elder, 1988
Europe	89.5 \pm 3.3 Ma	Glaucony	K-Ar	Elewaut <i>et al.</i> , 1982
Europe	89.8 \pm 3.6 Ma	Glaucony	K-Ar	Odin & Pomerol, 1982
Europe	90.0 \pm 1.0 Ma	Glaucony	K-Ar	Kreuzer <i>et al.</i> , 1982
Europe	90.0 \pm 1.6 Ma	Glaucony	K-Ar	Kreuzer <i>et al.</i> , 1982
Europe	90.4 \pm 2.0 Ma	Glaucony	Rb-Sr	Elewaut <i>et al.</i> , 1982
Europe	91.2 \pm 0.5 Ma	Glaucony	K-Ar	Kreuzer <i>et al.</i> , 1982
Western Interior	92.8 \pm 1.8 Ma	Biotite	K-Ar	Obradovich & Cobban, 1975
Europe	92.9 \pm 2.1 Ma	Glaucony	Rb-Sr	Elewaut <i>et al.</i> , 1982
Western Interior	93.7 \pm 1.8 Ma	Biotite	K-Ar	Obradovich & Cobban, 1975
Western Interior	96.6 \pm 4.8 Ma	Biotite	K-Ar	Obradovich & Cobban, 1975

from several sections on a traverse from Pueblo, Colorado, to south-central Utah (see Figures 2, 3). The best sanidines for dating were recovered from the Four Corners (FC) and Nipple Butte (NB) sections. Usable zircons and apatites were recovered from all of the sections. Figure 4 shows the lithostratigraphic and biostratigraphic positions of the ashes in the Four Corners section in the Bridge Creek Limestone Member equivalent to the Mancos Shale (Kauffman *et al.*, 1987; Hintze, 1988). The lowest ash, PBC-5, comes from the *Sciponoceras gracile* ammonite zone and is the equivalent of bed 69 of Kennedy & Cobban (1991). The *Sciponoceras gracile* zone in the Western Interior has been correlated

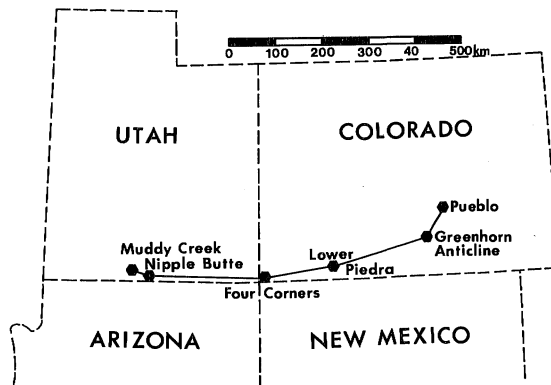


Figure 2. Locations of sections where Cenomanian-Turonian boundary ashes have been identified. The sections are described in detail in Elder & Kirkland (1985) and Kauffman *et al.* (1987).

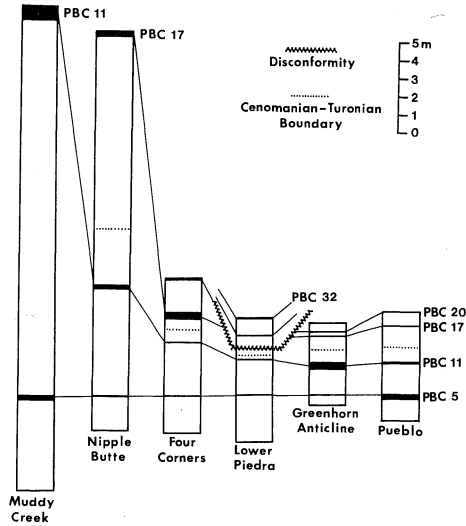


Figure 3. Relative position, correlation, and stratigraphic separation of ashes near the Cenomanian-Turonian boundary. Bentonites (black) are surrounded mostly by shales, limestones, and bentonitic clay, with some shell beds and nodule horizons (modified from Kauffman *et al.*, 1987).

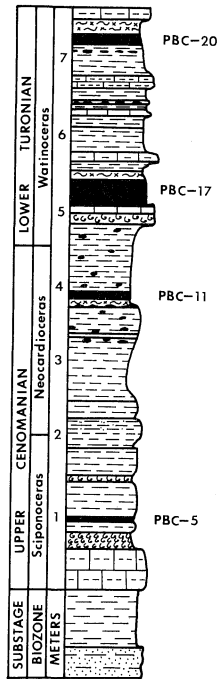


Figure 4. Detailed stratigraphic section of the Bridge Creek Limestone equivalent of the Mancos Shale from the Four Corners area showing the location of volcanic ash beds (black) in relation to ammonoid zones. Modified from Kauffman *et al.* (1987).

with the *Metoicoceras gestlinianum* zone in Europe (Kennedy, 1984). Ash PBC-11 (bed 80 of Kennedy & Cobban, 1991) is from the uppermost Cenomanian *Neocardioceras juddii* ammonite zone, and has been recognized in both North America and Europe (Kennedy, 1984). PBC-17 is located in the lower Turonian *Watinoceras devonense* ammonite zone (Kauffman *et al.*, 1987, Kennedy & Cobban, 1991) and is immediately above the first occurrence of the basal Turonian bivalve *Mytiloides* (Elder, 1988; Kennedy & Cobban, 1991). Ash PBC-20 did not contain datable minerals and will not be discussed further in the text.

The stratigraphic thickness from the lowest ash dated (PBC-5) to the highest ash dated (PBC-17) is about 4 m. Sample numbers used in the text include the section from which the sample was collected (NB or FC) and the ash bed number (PBC-5, PBC-11, or PBC-17). Additional detail on the lithostratigraphy and biostratigraphy of these sections can be found in Elder (1988), Elder & Kirkland (1985), Kauffman *et al.* (1987), and Kirkland (1991).

3. Petrology of the altered ash beds

The mineralogy, thickness (less than 50 cm) and wide distribution of beds PBC-5, PBC-11, and PBC-17 show that these smectite-rich units were once glass-rich pyroclastic ash fall deposits originating from large explosive eruptions. Consistent with their emplacement in quiet marine conditions (Elder, 1988), we detected no detrital minerals in PBC-11 and PBC-17; however, the PBC-5 sample from Nipple Butte (and at all other sections where it was sampled) contained apparently detrital garnet (Kowallis *et al.*, 1989), as well as detrital K-feldspar (see single-crystal $^{39}\text{Ar}/^{40}\text{Ar}$ results below). The garnet is rounded or fragmented and has a composition typical of metamorphic types. Both PBC-11 and PBC-17 had a magmatic mineral assemblage that included quartz, sanidine, plagioclase, biotite, zircon and apatite; they are essentially indistinguishable from one another on this basis. The PBC-5 ash is mineralogically distinctive, containing monazite and two populations of zircon (clear euhedral grains and pink subhedral grains) in addition to sanidine, plagioclase, quartz, biotite (commonly as vermiculite) and apatite. Zircons with abundant dark mineral inclusions are common in PBC-11 and PBC-17, but rare in the clear zircons of PBC-5, which contain irregularly shaped, elongate, transparent inclusions (glass?). The zircons from PBC-11 and PBC-17 are also indistinguishable morphologically from one another. According to the classification of Pupin (1980), zircons in PBC-11 have an average A index of 432 ± 9 (1σ) and a T index of 640 ± 7 , compared with 429 ± 10 and 644 ± 7 for PBC-17 (Figure 5). These values are characteristic of those found in calc-alkaline series granite rocks and their volcanic equivalents dacites and rhyolites (Figure 5). Subadjacent PBC-5, which contains monazite, has zircons that are morphologically distinctive from PBC-11 and PBC-17. Clear zircons from PBC-5 have an A index of about 397 ± 13 and a T index of 327 ± 9 (Figure 5), similar to those found in peraluminous granitic rocks (Kowallis *et al.*, 1989).

Samples of PBC-5 and PBC-11 were analyzed for major and trace element composition from six different locations to examine distinctiveness and homogeneity of the ash sheets. One sample of PBC-17 was analyzed from the Four Corners section. In general, the chemical analyses (Kowallis *et al.*, 1989) of the altered ashes substantiated the bed-by-bed correlations made by Kauffman *et al.*

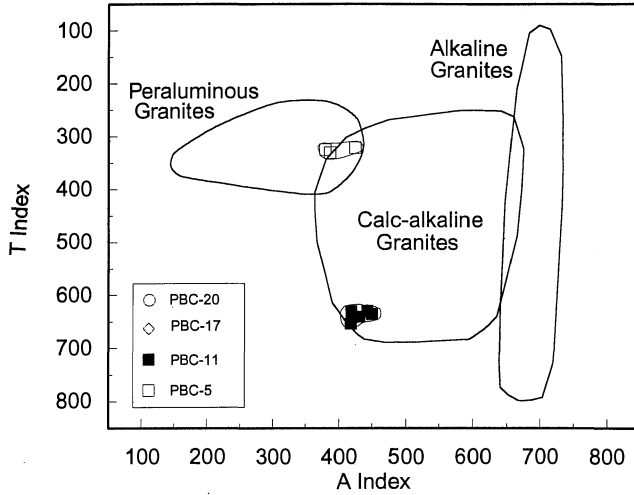


Figure 5. Average Pupin A and T zircon morphology indices for ashes PBC-5 (from 3 sections), PBC-11 (from 4 sections), PBC-17 (one sample) and PBC-20 (one sample), from near the Cenomanian-Turonian boundary. Samples from PBC-17 and PBC-20 ash beds are hidden by PBC-11 symbols. The lines about the points enclose two standard errors of the mean. Fields for various granite types are from Pupin (1980).

(1987) and Elder (1988) based on paleontology, physical and isotopic stratigraphy. Trace-element systematics (Figure 6) also suggest that the magmas were high K, calc-alkaline rhyolites erupted from a magmatic arc rooted in mature continental crust (Leat & Thorpe, 1986; Pearce *et al.*, 1984; Winchester & Floyd, 1977). Contemporaneous granitic plutons that might have fed these

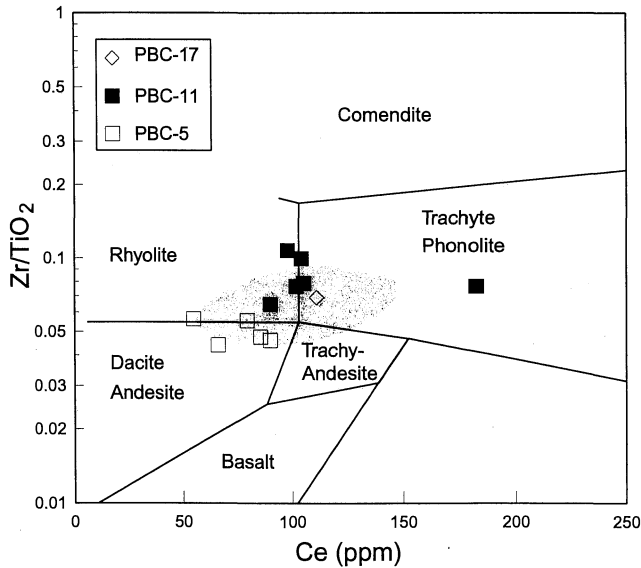


Figure 6. Classification diagram for strongly altered Cenomanian-Turonian ash beds based on immobile trace-element concentrations (Winchester & Floyd, 1977). Shaded area shows composition of fresh Tertiary rhyolites from the Indian Peak volcanic field (Best *et al.*, 1989). Scatter in the enclosed fields is the combined result of original magmatic variation, eruptive fractionation and bentonitic alteration, and gives a visual estimate of the amount of variation to be expected in a given ash bed. The Cenomanian-Turonian ashes were probably originally rhyolitic (see text).

eruptions are found in southern Arizona, the eastern Sierra Nevada and in the Idaho and Boulder batholiths (Christiansen *et al.*, 1994).

4. Geochronology of altered ash beds

Several isotopic dating methods at different laboratories were applied to the Cenomanian-Turonian samples. Each method and the results obtained are discussed in detail below.

4.1. $^{40}\text{Ar}/^{39}\text{Ar}$ dating methods

Single-crystal $^{40}\text{Ar}/^{39}\text{Ar}$ laser-fusion dating of sanidine. The $^{40}\text{Ar}/^{39}\text{Ar}$ age determinations were performed using an Ar-ion laser to fuse single crystals of irradiated sanidine for isotopic analysis (details of the methodology used here are provided in Deino & Potts, 1990, Deino *et al.*, 1990, and Chesner *et al.*, 1991). It should be emphasized, for comparison with the furnace step-heating experiments described later, that the laser-fusion dating procedure includes a low-power laser pre-heat of the samples under high vacuum. This step has proven to be an efficient means of driving away surficial argon prior to total fusion and analysis. This procedure, roughly equivalent to the preliminary degas procedure used with the furnace step-heating technique described later, results in markedly reduced atmospheric argon contamination and is probably also efficient in degassing alteration products that may be present on grain surfaces.

Samples were irradiated for 20 hours in the hydraulic rabbit of the Omega West research reactor, Los Alamos National Laboratory. Sanidine from the Fish Canyon Tuff (FCT) was employed as the neutron fluence monitor. We use a reference age for this sanidine of 27.84 Ma as determined by Cebula *et al.* (1986) by $^{40}\text{Ar}/^{39}\text{Ar}$ dating, using MMhb-1 hornblende as their monitor reference, but corrected for an updated laboratory-consensus conventional K–Ar age of MMhb-1 hornblende of 520.4 ± 1.7 Ma (Samson & Alexander, 1987). The age of this standard has been independently determined at the Institute of Human Origins using conventional K–Ar techniques and has verified this age, within error. We feel it is useful to adopt this published result until more precise and accurate absolute calibrations are available.

In our experiment, grains of MMhb-1 were co-mingled with the FCT sanidine in the same irradiation position and then analyzed as a cross-check on the neutron fluence determination. We obtained an age for MMhb-1 of 521.5 ± 0.9 Ma (weighted mean age and 1σ standard error of the weighted mean) using the FCT sanidine as a monitor (Table 2). This value is within 0.2% of, and is statistically indistinguishable from, the age of MMhb-1 given by Samson & Alexander (1987). In practice, we prefer to use the FCT sanidine as the irradiation monitor, because the sanidine can be analyzed with greater precision than the hornblende (about 0.1% s.e.m. compared with *c.* 0.2–0.3% s.e.m. for MMhb-1), and is more closely related in terms of argon isotopic compositions to the sanidine unknowns, particularly in measured $^{40}\text{Ar}/^{39}\text{Ar}$ and $^{37}\text{Ar}/^{39}\text{Ar}$ ratios.

We have propagated an uncertainty in \bar{f} of 0.3% into the weighted-mean age error calculations based on laboratory irradiation-to-irradiation reproducibility, which reflects both the error in measuring \bar{f} through repeated analyses of the monitor, and the uncertainty in relating the fluence of the monitor position to that of the unknowns.

A total of 87 single crystals of feldspar was analyzed from the three

Table 2. Sanidine single-crystal $^{40}\text{Ar}/^{39}\text{Ar}$ analytical data.

Lab ID#	Ca/K	$^{36}\text{Ar}/^{39}\text{Ar}$	$^{40}\text{Ar}^*/^{39}\text{Ar}$	^{40}Ar (Moles $\times 10^{13}$)	% $^{40}\text{Ar}^*$	Age (Ma) $\pm 1\sigma$
Sample FC-PBC-17						
2305B-01	0.0200	0.00019	3.580	0.3	98.4	94.25 \pm 0.48
2305B-02	0.0084	0.00013	3.543	0.4	98.9	93.29 \pm 0.35
2305B-03	0.0138	0.00010	3.530	0.2	99.2	92.96 \pm 0.62
2305B-04	0.0175	0.00021	3.553	0.3	98.3	93.54 \pm 0.42
2305B-07	0.0053	0.00012	3.544	0.3	99.0	93.31 \pm 0.48
2305B-11	0.0057	0.00025	3.561	0.3	98.0	93.76 \pm 0.49
2305B-12	0.0020	0.00005	3.575	0.2	99.6	94.12 \pm 0.68
2305B-13	0.0116	0.00024	3.550	0.2	98.0	93.48 \pm 0.60
2305B-15	0.0169	0.00026	3.579	0.3	97.9	94.23 \pm 0.49
2305B-16	0.0092	0.00028	3.487	0.1	97.7	91.85 \pm 0.96
2305B-18	0.0152	0.00018	3.559	0.3	98.5	93.71 \pm 0.45
2305B-19	0.0194	0.00031	3.507	0.3	97.5	92.37 \pm 0.42
Weighted mean age $\pm 1\sigma$ s.e.m (without error in J)=						93.46 \pm 0.19
(with error in J)=						\pm 0.26
Sample FC-PBC-11						
2303-01	0.0093	0.00001	3.544	4.4	99.9	93.31 \pm 0.21
2303-02	0.0078	0.00002	3.554	3.9	99.9	93.57 \pm 0.22
2303-03	0.0102	0.00004	3.555	4.9	99.7	93.61 \pm 0.21
2303-04	0.0116	0.00005	3.557	5.9	99.6	93.66 \pm 0.22
2303-05	0.0124	0.00008	3.546	4.2	99.3	93.37 \pm 0.24
2303-06	0.0115	0.00005	3.536	2.6	99.5	93.12 \pm 0.24
2303-07	0.0078	0.00002	3.559	1.9	99.8	93.71 \pm 0.26
2303-08	0.0095	0.00003	3.544	2.1	99.7	93.32 \pm 0.24
2303-09	0.0116	0.00006	3.561	1.6	99.5	93.76 \pm 0.27
2303-10	0.0122	0.00004	3.546	2.5	99.7	93.37 \pm 0.22
2303-11	0.0110	0.00005	3.538	1.7	99.6	93.16 \pm 0.24
2303-12	0.0105	0.00007	3.561	2.3	99.4	93.75 \pm 0.24
2303-13	0.0111	0.00004	3.525	2.8	99.7	92.84 \pm 0.22
2303-15	0.0112	0.00012	3.533	2.3	99.0	93.03 \pm 0.23
2303-16	0.0101	0.00020	3.529	1.0	98.4	92.93 \pm 0.30
2303-17	0.0133	0.00009	3.531	1.9	99.2	92.99 \pm 0.23
2303-18	0.0112	0.00004	3.550	3.7	99.7	93.46 \pm 0.21
2303-19	0.0111	0.00008	3.536	3.4	99.3	93.12 \pm 0.22
2303-20	0.0111	0.00005	3.563	3.6	99.5	93.80 \pm 0.22
2303-21	0.0119	0.00007	3.532	1.9	99.4	93.01 \pm 0.22
2303-23	0.0099	0.00004	3.527	3.1	99.7	92.89 \pm 0.21
2303-24	0.0125	0.00005	3.563	2.2	99.6	93.82 \pm 0.23
2303-25	0.0086	0.00010	3.551	1.8	99.2	93.51 \pm 0.24
2303-26	0.0092	0.00009	3.564	3.5	99.3	93.84 \pm 0.22
2303-27	0.0112	0.00006	3.549	3.2	99.5	93.44 \pm 0.21
2303-28	0.0112	0.00005	3.540	2.6	99.6	93.22 \pm 0.22
2303-29	0.0098	0.00010	3.533	1.7	99.1	93.04 \pm 0.24
2303-30	0.0125	0.00004	3.541	3.0	99.6	93.25 \pm 0.21
2303-31	0.0106	0.00005	3.516	2.3	99.6	92.59 \pm 0.22
Weighted mean age $\pm 1\sigma$ s.e.m (without error in J)=						93.33 \pm 0.06
(with error in J)=						\pm 0.25

Cenomanian-Turonian samples (FC-PBC-17, FC-PBC-11, NB-PBC-5). Of these, 32 were culled from the data set before calculation of mean eruption ages for one or more of the following criteria, listed in order of application:

(1) Markedly lower percentage of radiogenic argon (% $^{40}\text{Ar}^*$) relative to other “acceptable” analyses (i.e. less than 97% $^{40}\text{Ar}^*$), possibly reflecting alteration or the presence of inclusions. This applies to four analyses that would otherwise be analytically acceptable.

(2) Incomplete fusion or fusion of a very small crystal, resulting in unacceptably low gas yields, applicable to a handful of cases.

(3) Analytical difficulties (spectrometer signal instability or, in one case, a computer recording error) encountered during analysis of one unknown and three standard runs.

Table 2. (Continued).

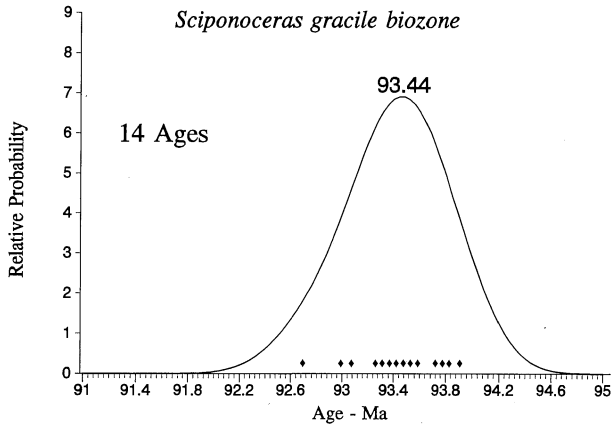
Lab ID#	Ca/K	$^{36}\text{Ar}/^{39}\text{Ar}$	$^{40}\text{Ar}^*/^{39}\text{Ar}$	^{40}Ar (Moles $\times 10^{13}$)	% $^{40}\text{Ar}^*$	Age (Ma) $\pm 1\sigma$
Sample NB-PBC-5						
2301-01	0.0129	0.00010	3.537	1.4	99.2	93.15 \pm 0.22
2301-05	0.0093	0.00006	3.549	2.9	99.5	93.46 \pm 0.21
2301-14	0.0097	0.00010	3.563	4.7	99.2	93.81 \pm 0.21
2301-15	0.0065	0.00006	3.555	2.2	99.5	93.61 \pm 0.22
2301-17	0.0099	0.00010	3.535	1.9	99.1	93.09 \pm 0.23
2301-18	0.0129	0.00015	3.552	3.4	98.8	93.53 \pm 0.22
2301-20	0.0154	0.00013	3.555	1.9	98.9	93.59 \pm 0.23
2301-22	0.0100	0.00004	3.545	1.3	99.7	93.36 \pm 0.23
2301-24	0.0135	0.00014	3.546	2.2	98.8	93.38 \pm 0.22
2301-25	0.0063	0.00005	3.567	1.0	99.5	93.90 \pm 0.26
2301-26	0.0078	0.00004	3.566	2.1	99.7	93.87 \pm 0.22
2301-29	0.0112	0.00011	3.552	1.9	99.1	93.52 \pm 0.24
2301-31	0.0085	0.00009	3.523	1.4	99.2	92.78 \pm 0.23
2301-35	0.0084	0.00004	3.571	1.6	99.7	94.01 \pm 0.23
Weighted mean age $\pm 1\sigma$ s.e.m (without error in J)=						93.50 \pm 0.19
(with error in J)=						± 0.30
Old contaminants, sample NB-PBC-5:						
2301-32	0.0122	0.00008	6.255	4.2	99.6	161.6 \pm 0.4
2301-07	0.0150	0.00015	6.395	4.5	99.3	165.0 \pm 0.4
2301-04	0.0071	0.00063	8.260	3.6	97.8	210.5 \pm 0.5
2301-21	0.0469	0.00070	9.740	3.2	97.9	245.7 \pm 0.6
2301-23	0.0050	0.00090	10.33	9.2	97.5	259.5 \pm 0.6
2301-28	0.0124	0.00040	12.58	8.7	99.1	311.5 \pm 0.7
2301-11	0.0017	0.00029	24.42	36.2	99.6	562.5 \pm 1.1
2301-03	0.0025	0.00029	26.72	23.6	99.7	607.4 \pm 1.3
2301-08	0.0161	0.00018	32.32	34.2	99.8	712.2 \pm 1.4
2301-34	0.0096	0.00039	33.36	40.3	99.7	731.3 \pm 1.5
2301-06	0.0119	0.00037	33.73	20.2	99.7	737.8 \pm 1.4
2301-10	0.0051	0.00034	37.61	32.8	99.7	806.2 \pm 1.5
2301-12	0.0040	0.00055	38.66	42.4	99.6	824.3 \pm 1.6
2301-16	0.0084	0.00064	50.21	43.0	99.6	1011.8 \pm 2.0
2301-09	0.0070	0.00036	51.81	62.4	99.8	1036.4 \pm 2.0
2301-19	0.0069	0.00024	56.25	94.4	99.9	1102.7 \pm 2.5
2301-36	0.0039	0.00038	57.15	92.5	99.8	1115.8 \pm 2.1
2301-13	8.0320	0.00770	75.86	1.0	97.5	1369.5 \pm 3.2

Notes: Errors in age quoted for individual runs are 1σ analytical uncertainty. Weighted averages are calculated using the inverse variance as the weighting factor (Taylor, 1982). Errors in the weighted averages are 1σ standard error of the mean (Samson & Alexander, 1987). Ca/K is calculated from $^{37}\text{Ar}/^{39}\text{Ar}$ using a multiplier of 1.96. $^{40}\text{Ar}^*$ refers to radiogenic argon. 'Moles ^{40}Ar ' refers to the estimated total moles of ^{40}Ar released during fusion based on spectrometer sensitivity considerations. $\lambda = 5.543 \times 10^{-10} \text{ y}^{-1}$. Isotopic interference corrections; $(^{36}\text{Ar}/^{37}\text{Ar})_{\text{Ca}} = (2.58 \pm 0.06) \times 10^{-4}$, $(^{39}\text{Ar}/^{37}\text{Ar})_{\text{Ca}} = (6.7 \pm 0.3) \times 10^{-4}$, $(^{40}\text{Ar}/^{39}\text{Ar})_{\text{K}} = (8 \pm 7) \times 10^{-4}$. $J = 0.01498 \pm 0.00004$.

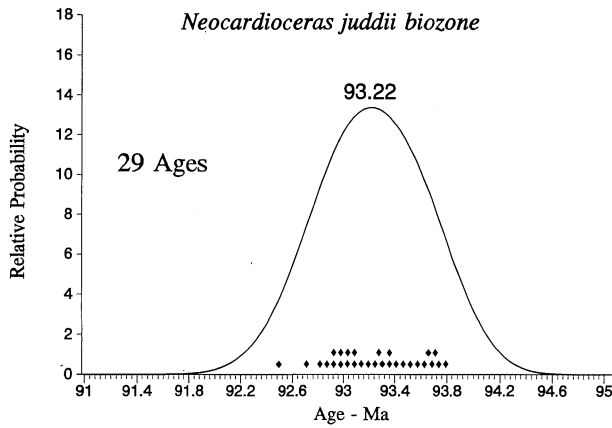
(4) Markedly old age, obviously indicating origin as a xenocrystic or detrital contaminant feldspar. Such grains, found only in sample NB-PBC-5, ranged in age from 110 to 1369 Ma.

The filtered data set yields weighted mean single-crystal ages for the three samples, from stratigraphically oldest to youngest, of 93.50 ± 0.52 Ma (2σ standard error of the mean, incorporating error in J) for NB-PBC-5, 93.33 ± 0.50 Ma for FC-PBC-11 and 93.46 ± 0.6 Ma for FC-PBC-17. The uncertainty of the mean age of this last sample is greater than the others as a consequence of the smaller grain size (about one-tenth the volume of NB-PBC-5 and FC-PBC-11 grains) leading to greater imprecision of measurement of the argon ion beams, and also because fewer crystals were available for dating.

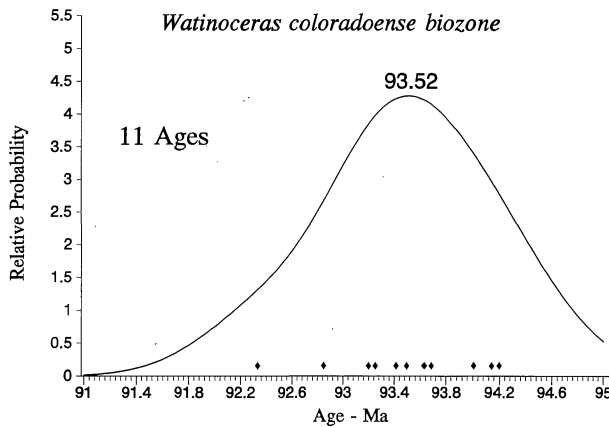
The culled single-grain analyses yield nearly symmetrical gaussian-like age-probability distributions (Table 2; Figure 7). These age-probability graphs provide an important tool for assessing whether subtle contamination remains in



(a)



(b)



(c)

Figure 7. Single-crystal laser-fusion $^{40}\text{Ar}/^{39}\text{Ar}$ dating results represented as age-probability distributions for samples A, PBC-5, B, PBC-11, and C, PBC-17. Distributions are calculated by the methods described in Hurford *et al.* (1984) and Kowallis *et al.* (1986). Diamonds show the individual grain ages used in producing the plots. Numbers above the curves are the peak values or age modes.

the data set. For all three samples the absence of multimodality or strongly skewed distributions suggests that all grains are of primary origin within the resolution of the technique. Medians and modes of the populations, two indicators of central tendency that are relatively unaffected by outliers or skewed populations, are in agreement with the weighted mean ages. The medians are virtually identical in age (93.53, 93.32, 93.51 Ma, respectively), while the modes (Figure 7) fall within about 0.1% of the mean ages (93.47, 93.22, and 93.52 Ma).

⁴⁰Ar/³⁹Ar age spectrum dating of sanidine. High-precision ⁴⁰Ar/³⁹Ar age-spectrum dating of two sanidine samples (FC-PBC-11 and FC-PBC-17) was performed using a low-blank, double-vacuum resistance furnace similar in design to that described by Staudacher *et al.* (1978) for step-heating. Before analysis the samples were irradiated for 20 hours in the central thimble facility of the US Geological Survey TRIGA reactor (Dalrymple *et al.*, 1981). After irradiation the samples were returned to the US Geological Survey Isotope Geology laboratory in Reston and analyzed for their argon isotopic composition using a V.G. MM1200b rare-gas mass spectrometer operated in the static mode. Details of the analytical procedure can be found in Wintsch *et al.* (1991). The only variation from this procedure was in the measurement of ³⁶Ar. In this study we collected data for four, five-second intervals for ³⁶Ar peak and background measurements in each of the five measurement cycles and averaged these values accordingly. This allowed for the use of standard linear regression statistical techniques in calculating ³⁶Ar values and greater precision in these measurements. Data reduction was accomplished using an updated version of the computer program ArAr* (Haugerud & Kunk, 1988) using the decay constants recommended by Steiger & Jäger (1977). The primary monitor used for the irradiation was FCT-3 sanidine from the Fish Canyon Tuff. *J* values were interpolated from replicate measurements of individual monitors. The US Geological Survey laboratory in Reston routinely uses an age of 27.79 Ma for FCT-3 (Kunk *et al.*, 1985; Cebula *et al.*, 1986) compared against MMhb-1 hornblende at an age of 519.4 ± 2.4 Ma (Alexander *et al.*, 1978 and Dalrymple *et al.*, 1981), because of the questions concerning the precision of the more recently published age of 520.4 ± 1.7 Ma (Samson & Alexander, 1987), given the 2% spread in their data. However, for ease of comparison with the laser-fusion data, we have reduced the age spectrum data using an age of 27.84 Ma for FCT-3 sanidine against MMhb-1 at 520.4 ± 1.7 Ma. We have included (parenthetically) plateau and total-gas ages that have been calculated using an age of 27.79 Ma for FCT-3 sanidine for comparison with other data from the Reston argon lab.

In addition to determining a high-precision age for samples FC-PBC-11 and FC-PBC-17, a primary objective of ⁴⁰Ar/³⁹Ar age-spectrum dating was to determine if their argon systems had been disturbed in any way. ⁴⁰Ar/³⁹Ar laser-fusion dating of these samples detected no sanidine or other K-feldspar contaminant, although this procedure would not necessarily detect contaminants present in quantities of a few percent or less. The mineral separates used for our analyses were greater than 99.9% sanidine, with the chief contaminate being inclusions contained within individual sanidine grains. With this exception the ⁴⁰Ar/³⁹Ar age spectra of these samples should represent data from a single component sanidine system. If the age spectrum of each sample is undisturbed then all of the temperature steps should agree in age within the limits of

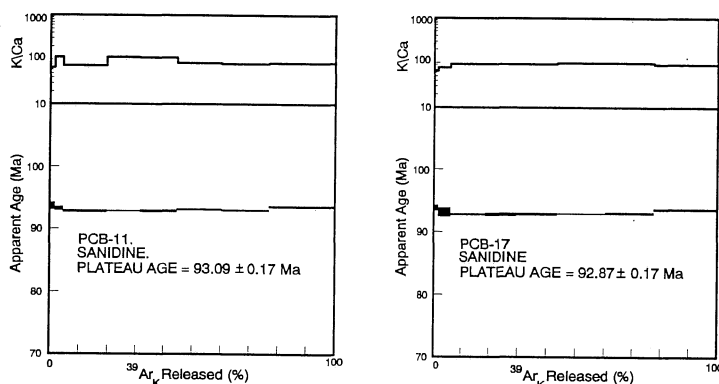


Figure 8. $^{40}\text{Ar}/^{39}\text{Ar}$ age spectra and K/Ca plots for PBC-11 and PBC-17.

analytical precision. In this case the samples should have plateau ages which include 100% of the argon released.

In both samples (Figure 8, Table 3), a slight disturbance in the age spectrum

Table 3. $^{40}\text{Ar}/^{39}\text{Ar}$ age spectrum data.

T (°C)	% ^{39}Ar of Total	$^{40}\text{Ar}_R/^{39}\text{Ar}_K^*$	Apparent K/Ca†	Radiogenic K/Cl	Radiogenic yield (%)	$^{39}\text{Ar}_K \ddagger$ ($\times 10^{-12}$ moles)	Apparent age§ \pm precision (Ma)
FC-PBC-11 Sanidine J = 0.005089 \pm 0.20%							
Sample wt. = 0.1903 g							
950	1.6	10.477	66.4	****	95.8	0.532	93.83 \pm 0.29
1050	2.9	10.428	113.8	****	98.3	0.967	93.40 \pm 0.16
1150	15.1	10.376	73.7	****	99.5	4.997	92.95 \pm 0.10
1200	11.9	10.384	114.7	****	99.6	3.919	93.02 \pm 0.04
1250	13.0	10.386	112.4	****	99.5	4.296	93.04 \pm 0.09
1300	15.7	10.413	83.7	****	99.5	5.177	93.27 \pm 0.06
1350	16.4	10.399	81.6	****	99.2	5.410	93.19 \pm 0.06
1450	23.3	10.464	85.1	****	99.0	7.689	93.72 \pm 0.08
Total gas		K/Ca	90.2				Age 93.17 \pm 0.08 (93.01 \pm 0.17)
Plateau age (72.1% of gas in 1150–1350°C steps)							
93.09 \pm 0.17 (92.95 \pm 0.17)							
FC-PBC-17 Sanidine J = 0.005098 \pm 0.20%							
Sample wt. = 0.1264 g							
950	1.6	10.475	64.7	6702	96.4	0.292	93.81 \pm 0.21
1050	4.4	10.395	76.9	****	99.3	0.828	93.12 \pm 0.34
1150	12.6	10.356	93.0	****	99.5	2.364	92.77 \pm 0.06
1200	11.0	10.354	92.8	****	99.4	2.063	92.76 \pm 0.12
1250	13.9	10.363	93.4	****	99.7	2.613	92.84 \pm 0.09
1300	16.9	10.370	98.3	****	99.6	3.175	92.90 \pm 0.04
1350	17.3	10.377	97.1	****	99.6	3.329	92.96 \pm 0.07
1450	22.3	10.452	90.8	****	99.6	4.183	93.62 \pm 0.08
Total gas		K/Ca	93.0				Age 92.98 \pm 0.17 (92.82 \pm 0.17)
Plateau age (76.1% of gas in 1050–1350°C steps)							
92.87 \pm 0.17 (92.71 \pm 0.17)							

* This ratio has been corrected for mass discrimination, atmospheric argon, and the production of interfering isotopes during irradiation using the values reported by Dalrymple *et al.* (1981) for $(^{36}\text{Ar}/^{37}\text{Ar})_{\text{Ca}}$, $(^{39}\text{Ar}/^{37}\text{Ar})_{\text{Ca}}$, and $(^{40}\text{Ar}/^{39}\text{Ar})_{\text{K}}$.

† Apparent K/Ca ratios were calculated using the equation given in Fleck *et al.* (1977).

‡ ^{39}Ar concentrations were calculated using the measured sensitivity of the mass spectrometer and have a precision of about 5%.

§ Comparisons between steps for the determination of the existence of an age plateau were done using the larger of: the calculated uncertainty from the analyses or, the reproducibility limit of the mass spectrometer as determined by replicate measurements of FCT-3. During the period of time in which these samples were analyzed the reproducibility limit was 0.15%.

can be observed in both the lowest and highest temperature release steps, with those ages being somewhat older than the bulk of the gas. The majority of the gas in both samples (72.1% for FC-PBC-11 in the 1200 to 1450°C steps and 76.1% for FC-PBC-17 in the 1050 to 1350°C steps) agrees in age, within the limits of analytical precision, and forms an age plateau as defined by Fleck *et al.* (1977) of 93.09 ± 0.17 Ma for FC-PBC-11 and 92.87 ± 0.17 Ma for FC-PBC-17. Total gas ages for both samples, 93.17 Ma for FC-PBC-11 and 92.98 Ma for FC-PBC-17, although marginally higher, agree with the plateau ages within the limits of analytical precision.

The disturbances in both of the age spectra are minor and the cause of these disturbances cannot be discerned with any degree of certainty. While the overall pattern of the age spectra could be interpreted to represent the presence of extraneous argon, variations in the apparent K/Ca and K/Cl ratios of both samples suggest that slight impurities contained as inclusions within individual grains may account for these variations in age. Isotope correlation analysis of the samples does little to resolve this question, because of the high radiogenic yield of all steps in the age spectra, except those with K/Ca and K/Cl ratios that may represent included impurities within the samples. An inverse isotope correlation diagram of the data for FC-PBC-17 (Figure 9) readily demonstrates this problem. With the exception of point A, which has somewhat lower K/Ca ratios than the rest of steps, all of the data points cluster tightly together near the $^{39}\text{Ar}/^{40}\text{Ar}$ axis. A line regressed through all of the steps in the analysis suggests an initial $^{40}\text{Ar}/^{36}\text{Ar}$ ratio of 381 ± 33 and an age of 92.85 ± 0.29 Ma. This initial $^{40}\text{Ar}/^{36}\text{Ar}$ ratio could be interpreted to represent the presence of a slight amount of excess argon in the sample, in which case the age calculated from this diagram of 92.88 ± 0.30 Ma would represent the apparent age of the sample. However, both the age and initial $^{40}\text{Ar}/^{36}\text{Ar}$ ratio are controlled primarily by point A with its lower K/Ca ratio. If point A is dropped from the correlation, the initial $^{40}\text{Ar}/^{36}\text{Ar}$ ratio increases to 2013 ± 7158 , and the age decreases to 90.51 ± 10.70 Ma. These numbers are lacking in resolution and are not different from the modern day $^{40}\text{Ar}/^{36}\text{Ar}$ value of 295.5 and the plateau age for this sample, respectively.

A comparison of the plateau and correlation ages shows that neither one is resolvable from the other. We prefer, however, the plateau age of the samples because of the demonstrated within sample reproducibility for the apparent ages

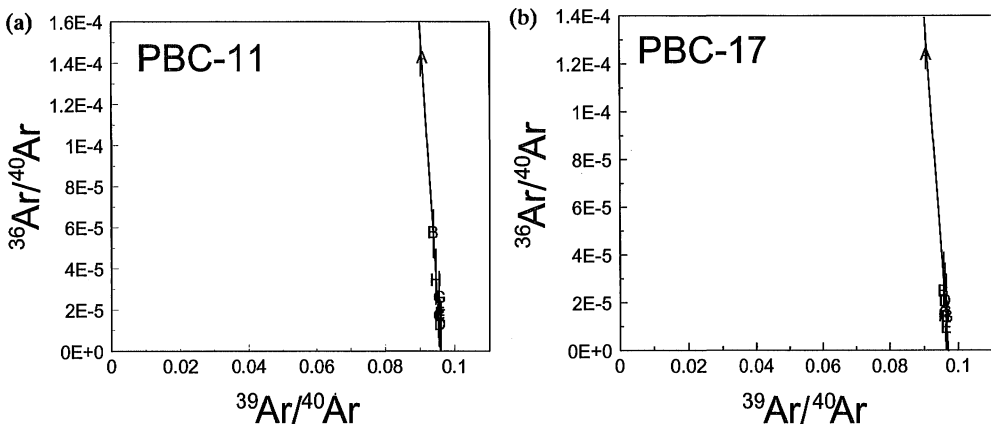


Figure 9. Inverse correlation diagrams from age spectra analyses. For A, PBC-11: age = 92.85 ± 0.29 Ma, initial $^{40}\text{Ar}/^{36}\text{Ar} = 381 \pm 33$, and MSWD = 0.307. For B, PBC-17: age = 93.04 ± 0.26 Ma, initial $^{40}\text{Ar}/^{36}\text{Ar} = 360 \pm 32$, and MSWD = 0.279.

of steps within that portion of the age spectra, and because they exclude steps in which the ages may be older due to the presence of included impurities within individual sanidine grains.

Comparison of bulk $^{40}\text{Ar}/^{39}\text{Ar}$ age spectrum and single-crystal laser-fusion results. It is not clear whether the total-gas spectrum ages or the plateau ages of the incremental-release furnace experiments are most directly comparable to the laser-fusion results. If the source of the discordance observed in the step-heating spectra of both samples is a feature present in each grain, or even more or less homogeneously distributed in small populations of grains, then the laser-fusion results would be most comparable with the total-gas ages. If, on the other hand, the source of the older ages in the final portions of the step heating spectra are due to relatively rare inclusions or xenocrystic (refractory) feldspar, then the hand-picked small-population sampling of the laser-fusion experiment may have avoided such aberrant ages and so these data are best compared with the plateau ages.

The appropriate statistical test to employ for comparing the ages between the different dating methods is one based on heterogeneity of variances, since the variances are derived from quite different kinds of experiments without expectation that they should be directly comparable. We have employed a t' test assuming heterogeneity of variances using Satterthwaite's (1946) solution to obtain an evaluation of the number of degrees of freedom. At $\alpha = 0.05$, this test reveals no significant difference in the plateau or total-gas ages compared to the mean of the laser-fusion ages for PBC-11, and between the total-gas and laser-fusion mean for sample PBC-17. However, there is a statistically detectable difference between the plateau and the laser-fusion mean age for PBC-17.

This age difference may be due to systematic inter-laboratory bias, as suggested by the fact that the GC/IHO results for all samples are consistently older than those obtained at the USGS/Reston by about 0.5 Ma. Alternatively, the implication of this comparison may be that the source of discordance is homogeneously distributed, thus adversely influencing the laser-fusion results.

4.2. U–Pb zircon dating

The zircon population in these two samples generally consisted of colorless prisms (3:1 length:width ratios) or fragments that contained abundant fluid and mineral inclusions. Most zircon crystals selected for analysis contained a few or no visible inclusions. All five zircon fractions listed in Table 4 were given an air abrasion treatment following the procedure outlined by Krogh (1982) to eliminate the outer portions of the grains that typically experience Pb loss. Isolation of Pb and U from zircon using anion exchange chromatography generally followed the procedure of Krogh (1973). The concentrations of Pb and U were determined by isotope dilution using a mixed ^{235}U – ^{205}Pb tracer solution. Both Pb and U were loaded together onto outgassed, single Re filaments in a silica gel–phosphoric acid mixture (Cameron *et al.*, 1969) and the isotopic compositions were determined on a VG354 solid source mass spectrometer in single collector mode. All isotopic data were measured using a Faraday or Daly photomultiplier detector and have been corrected for mass discrimination (1‰/amu). In addition, a Daly/Faraday conversion factor of 4‰/amu has been applied to all Daly data. The errors reported in Table 4 are quoted at one sigma and were calculated by propagating all known sources of error. The age uncertainties are reported as two sigma errors. The ^{238}U and ^{235}U decay

Table 4. U-Pb Zircon results for Cenomanian-Turonian bentonites.

Description: sample fraction number	Weight of sample (μg)	Concentration				Atomic ratios \ddagger				Age \pm error (Ma)		
		U (ppm)	Pb (ppm)	Th \dagger (ppm)	Common Pb(pg)	$^{206}\text{Pb}/^{204}\text{Pb}$	$^{206}\text{Pb}/^{238}\text{U}$	$^{207}\text{Pb}/^{235}\text{U}$	$^{207}\text{Pb}/^{206}\text{Pb}$	$^{206}\text{Pb}/^{238}\text{U}$	$^{207}\text{Pb}/^{235}\text{U}$	
FC-PBC-11												
1	Z, (300)	228	469	7.1	225	19	5,884	0.01458 ± 3	0.09639 ± 20	0.04797 ± 6	93.3 ± 0.2	93.4 ± 0.2
2	Z, (60)	49	364	5.5	167	4	8,503	0.01462 ± 2	0.09660 ± 12	0.04793 ± 3	93.6 ± 0.1	93.6 ± 0.1
3	Z, (152)	181	586	9.2	271	30	4,009	0.01494 ± 2	0.10092 ± 13	0.04898 ± 3	95.6 ± 0.1	97.6 ± 0.1
FC-PBC-17												
4	Z, (105)	96	548	8.4	216	5	18,548	0.01503 ± 3	0.10525 ± 19	0.05080 ± 3	96.2 ± 0.2	101.6 ± 0.2
5	Z, (25)	21	552	8.1	186	3	15,140	0.01468 ± 2	0.09717 ± 11	0.04800 ± 4	94.0 ± 0.1	94.2 ± 0.1

* Z = zircon (number of grains).

\dagger Th concentration estimated from the abundance of ^{208}Pb and U-Pb age.

\ddagger Atomic ratios corrected for blank (2pg Pb; 1pg U), fractionation (+0.1%/amu) and initial common Pb (Stacey & Kramers, 1975).

constants of $1.55125 \times 10^{-10} \text{ year}^{-1}$ and $9.8485 \times 10^{-10} \text{ year}^{-1}$, respectively and the isotopic composition of uranium ($^{238}\text{U}/^{235}\text{U} = 137.88$) are the values recommended by Jaffey *et al.* (1971).

The U–Pb results for three multi-grain fractions from sample FC-PBC-11 and two multi-grain fractions from sample FC-PBC-17 are presented in Table 4. The uranium content of all zircon fractions is moderately high (364–586 ppm) and the high $^{206}\text{Pb}/^{204}\text{Pb}$ ratios (>4000) indicate that the correction for initial common Pb is negligible. Two fractions (#1 and 2; Table 4) from FC-PBC-11 have identical apparent $^{206}\text{Pb}/^{238}\text{U}$ and $^{207}\text{Pb}/^{235}\text{U}$ ages with an average of $93.5 \pm 0.4 \text{ Ma}(2\sigma)$, and this age is interpreted as the best estimate for the zircon crystallization age. The other fraction (#3) analyzed from this sample has a slightly older age and U–Pb apparent ages that are not in agreement (i.e. 95.6 and 97.6 Ma). These older ages are interpreted as indicating the presence of an inherited-Pb component that could be present as invisible zircon cores or as older discrete zircon crystals that were accidentally incorporated into the fraction because of their morphological similarity to the younger grains.

A similar pattern in the U–Pb zircon results is observed for sample FC-PBC-17. Fraction #5 (Table 4) has similar $^{206}\text{Pb}/^{238}\text{U}$ and $^{207}\text{Pb}/^{235}\text{U}$ ages of 94.0 and 94.2 Ma respectively, and the average age of 94.1 Ma could be interpreted as the crystallization age of the zircon in this sample. Alternatively, this fraction may have a trace of inherited-Pb, as is more clearly the case with fraction #4, in which case the zircon crystallization age could be slightly younger than 94.0 Ma; this is consistent with the stratigraphic position of these two samples (see Figure 4). Although visible zircon cores were not detected, there is an indication that the amount of inherited-Pb component correlates with the abundance of inclusions as fractions #3 and #4 contained some grains with inclusions.

4.3. Fission track data

Apatites and zircons extracted from ashes PBC-11 and PBC-5 at several localities were dated using the external detector method. Ages were calculated using a zeta value of $11\,800 \pm 700$, determined from several irradiations of SRM-963 glass along with zircons and apatites from the Mt. Dromedary intrusion in eastern Australia. The errors for the ages were determined using the method described by Green (1981). The age data are shown in Table 5. Apatite

Table 5. Fission track age data.

Sample number	Mineral analyzed	No. of grains	Track density $\text{tr}/\text{cm}^2 \times 10^6$		Neutron detector tr/cm^2	Age (Ma) \pm error (2σ)
			Fossil	Induced		
MC-PBC-11	Zircon	5	13.54 (1895)*	10.04 (1406)*	11 922 (2327)*	$94 \pm 8 \text{ Ma}$
FC-PBC-11	Zircon	4	14.44 (1531)	11.23 (1190)	11 922 (2327)	$90 \pm 8 \text{ Ma}$
FC-PBC-11	Apatite	8	0.66 (1069)	0.80 (1301)	18 668 (3644)	$90 \pm 8 \text{ Ma}$
GA-PBC-11	Zircon	2	15.24 (1372)	10.99 (989)	11 922 (2327)	$97 \pm 9 \text{ Ma}$
P-PBC-11	Zircon	2	13.19 (1438)	10.10 (1101)	11 922 (2327)	$97 \pm 8 \text{ Ma}$
NB-PBC-5	Zircon	5	16.10 (1610)	11.69 (1169)	11 922 (2327)	$96 \pm 8 \text{ Ma}$
NB-PBC-5	Apatite	12	0.56 (711)	0.68 (869)	18 668 (3644)	$90 \pm 10 \text{ Ma}$
FC-PBC-5	Zircon	6	15.64 (1548)	12.03 (1191)	11 922 (2327)	$91 \pm 8 \text{ Ma}$
GA-PBC-5	Zircon	5	15.45 (1282)	11.64 (966)	11 922 (2327)	$93 \pm 9 \text{ Ma}$
P-PBC-5	Zircon	6	15.00 (1530)	11.21 (1143)	11 922 (2327)	$94 \pm 8 \text{ Ma}$

* Numbers in parenthesis represent track counts.

- Elder, W. P. & Kirkland, J. I. 1985. Stratigraphy and depositional environments of the Bridge Creek Limestone Member of the Greenhorn Limestone at Rock Canyon Anticline near Pueblo, Colorado. In *Fine-grained deposits and biofacies of the Cretaceous Western Interior Seaway: evidence of cyclic sedimentary processes*, Society of Economic Paleontologists and Mineralogists Field Trip Guidebook 4, 122–134.
- Elewaut, E., Keppens, E., Pasteels, P. & Robaszynski, F. (1982). NDS 81. In *Numerical dating in stratigraphy* (ed. Odin, G. S.), pp. 743–744 (John Wiley & Sons, Chichester, England).
- Fleck, R. J., Sutter, J. F. & Elliot, D. H. (1977). Interpretation of discordant $^{40}\text{Ar}/^{39}\text{Ar}$ age spectra of Mesozoic tholeiites from Antarctica. *Geochimica et Cosmochimica Acta* 41, 15–32.
- Gleadow, A. J. W., Duddy, I. R., Green, P. F. & Lovering, J. F. 1986. Confined fission track lengths in apatite: a diagnostic tool for thermal history analysis. *Contributions to Mineralogy and Petrology* 94, 405–415.
- Green, P. F. 1981. A new look at statistics in fission track dating. *Nuclear Tracks* 5, 77–80.
- Harland, W. B., Cox, A. V., Llewellyn, P. G., Picton, C. A. G., Smith, A. G. & Walters, R. 1982. *A geological time scale*, 128 pp. (Cambridge University Press, Cambridge).
- Harland, W. B., Armstrong, R. L., Cox, A. V., Craig, L. E., Smith, A. G. & Smith, D. G. 1990. *A geological time scale 1989*, 263 pp. (Cambridge University Press, Cambridge).
- Hattin, D. E. 1971. Widespread, synchronously deposited, burrow-mottled limestone beds in Greenhorn Limestone (Upper Cretaceous) of Kansas and southeastern Colorado. *Bulletin of the American Association of Petroleum Geologists* 55, 412–431.
- Hattin, D. E. 1975. Stratigraphy and depositional environment of Greenhorn Limestone (Upper Cretaceous) of Kansas. *Kansas University, Geological Survey Bulletin* 209, 128 pp.
- Hattin, D. E. 1979. Regional stratigraphy of limestone marker beds in Bridge Creek Limestone (Upper Cretaceous), Western Interior United States. *Bulletin of the American Association of Petroleum Geologists* 63, 464.
- Hattin, D. E. 1985. Distribution and significance of widespread, time parallel pelagic limestone beds in Greenhorn Limestone (Upper Cretaceous) of the central Great Plains and southern Rocky Mountains. *Society of Economic Paleontologists and Mineralogists, Guidebook* 4, 28–37.
- Haugerud, R. A. & Kunk, M. J. 1988. ArAr*, a computer program for reduction of ^{40}Ar – ^{39}Ar data. *U.S. Geological Survey Open File Report* 88–261, 68 pp.
- Hintze, L. F. 1988. Geologic History of Utah. *Brigham Young University Geology Studies, Special Publication* 7, 202 pp.
- Hurford, A. J., Fitch, F. J. & Clarke, A. 1984. Resolution of the age structure of the detrital zircon populations of two Lower Cretaceous sandstones from the Weald of England by fission track dating. *Geological Magazine* 121, 269–277.
- Jaffey, A. H., Flynn, K. F., Glendenin, L. E., Bentley, W. C. & Essling, A. M. 1971. Precision measurement of half-lives and specific activities of ^{235}U and ^{238}U . *Physical Review C* 4, 1889–1906.
- Kauffman, E. G. 1984. The fabric of Cretaceous marine extinctions. In *Catastrophes and earth history—the new uniformitarianism* (eds Berggren, W. A. & Van Couvering, J.), pp. 151–246 (Princeton University Press, Princeton, New Jersey).
- Kauffman, E. G., Sageman, B. B., Gustason, E. R. & Elder, W. P. 1987. High-resolution event stratigraphy, Greenhorn Cyclothem (Cretaceous: Cenomanian–Turonian), Western Interior Basin of Colorado and Utah. *Field Trip Guidebook, Rocky Mountain Section Geological Society of America*, 198 pp. (Geological Society of America, Boulder).
- Kennedy, W. J. 1984. Ammonite faunas and the ‘standard zones’ of the Cenomanian to Maastrichtian stages in their type areas, with some proposals for the definition of the stage boundaries by ammonites. *Bulletin of the Geological Society of Denmark* 33, 147–161.
- Kennedy, W. J. & Cobban, W. A. 1991. Stratigraphy and interregional correlation of the Cenomanian–Turonian transition in the Western Interior of the United States near Pueblo, Colorado, a potential boundary stratotype for the base of the Turonian stage. *Newsletters on Stratigraphy* 24, 1–33.
- Kennedy, W. J. & Odin, G. S. 1982. The Jurassic and Cretaceous time scale in 1981. In *Numerical dating in stratigraphy* (ed. Odin, G. S.), pp. 557–592 (Wiley-Interscience, New York).
- Kent, D. V. & Gradstein, F. M. 1986. A Jurassic to recent chronology. In *The geology of North America Volume M, the Western Atlantic region* (eds Tucholke, B. E. & Vogt, P. G.), pp. 45–50 (Geological Society of America, Boulder).
- Kirkland, J. I. 1991. Lithostratigraphic and biostratigraphic framework for the Mancos Shale (late Cenomanian to middle Turonian) at Black Mesa, northeastern Arizona. In *Stratigraphy, depositional environments, and sedimentary tectonics of the western margin Cretaceous Western Interior Seaway* (eds Nations, J. D. & Eaton, J. G.), *Geological Society of America, Special Paper* 260, 85–111.
- Kowallis, B. J., Christiansen, E. H. & Deino, A. 1989. Multi-characteristic correlation of Upper Cretaceous volcanic ash beds from southwestern Utah to central Colorado. *Utah Geological and Mineral Survey, Miscellaneous Publication* 89–5, 22 pp.
- Kowallis, B. J., Christiansen, E. H. & Deino, A. L. 1990. Age of the Cenomanian–Turonian

- boundary in the Western Interior of the United States. *Geological Society of Australia, Abstracts* 27, 55.
- Kowallis, B. J., Christiansen, E. H., Deino, A. L., Kunk, M. J. & Heaman, L. M. 1992. Age of the Cenomanian–Turonian boundary in the Western Interior of the United States. *Abstracts of 29th International Geological Congress, Kyoto, Japan* 1, 88.
- Kowallis, B. J., Heaton, J. S. & Bringham, K. 1986. Fission-track dating of volcanically derived sedimentary rocks. *Geology* 14, 19–22.
- Kreuzer, H., Čepek, P., Seibertz, E. & Weiss, W. L. 1982. NDS 226. In *Numerical dating in stratigraphy* (ed. Odin, G. S.), pp. 903–906 (John Wiley & Sons, Chichester, England).
- Korh, T. E. 1973. A low-contamination method for hydrothermal decomposition of zircon and extraction of U and Pb for isotopic age determinations. *Geochimica et Cosmochimica Acta* 37, 485–494.
- Krogh, T. E. 1982. Improved accuracy and U–Pb zircon ages by the creation of more concordant systems using an air abrasion technique. *Geochimica et Cosmochimica Acta* 46, 637–649.
- Kunk, M. J., Sutter, J. F. & Naeser, C. W. 1985. High-precision $^{40}\text{Ar}/^{39}\text{Ar}$ ages of sanidine, biotite, hornblende, and plagioclase from the Fish Canyon Tuff, San Juan Volcanic Field, south-central Colorado. *Geological Society of America, Abstracts With Programs* 17, 636.
- Lanphere, M. A. & TAILLEUR, I. L. 1983. K–Ar ages of bentonites in the Seabee Formation, northern Alaska: a late Cretaceous (Turonian) time-scale point. *Cretaceous Research* 4, 361–370.
- Leat, P. T. & Thorpe, R. S. 1986. Geochemistry of an Ordovician basalt-trachybasalt-subalkaline/peralkaline rhyolite association from the Llyn Peninsula, North Wales, UK. *Geological Journal* 21, 29–43.
- Obradovich, J. D. 1988. A different perspective on glauconite as a chronometer for geologic time scale studies. *Paleoceanography* 3, 757–770.
- Obradovich, J. D. 1991. A revised Cenomanian–Turonian time scale based on studies from the Western Interior United States. *Geological Society of America, Abstracts with Programs* 23, A296.
- Obradovich, J. D. 1992. A time scale for the Cretaceous. In *Mesozoic of the Western Interior, Society of Sedimentary Geology 1992 Theme Meeting, Abstracts*, 51.
- Obradovich, J. D. 1994. A Cretaceous time scale. In *Evolution of the Western Interior Basin* (eds Caldwell, W. G. E. & Kauffman, E. G.), *Geological Association of Canada Special Paper* 39, 379–396.
- Obradovich, J. D. & Cobban, W. A. 1975. A time-scale for the Late Cretaceous of the Western Interior of North America. *Geological Association of Canada, Special Paper* 13, 31–54.
- Odin, G. S. (ed.) 1982. *Numerical dating in stratigraphy*, Parts I and II, 1040 pp. (John Wiley & Sons, Chichester, England).
- Odin, G. S. & Pomerol, B. 1982. NDs 59. In *Numerical dating in stratigraphy* (ed. Odin, G. S.), pp. 719–720 (John Wiley & Sons, Chichester, England).
- Palmer, A. R. 1983. The Decade of North American Geology 1983 geologic time scale. *Geology* 11, 503–504.
- Pearce, J. A., Harris, N. B. W. & Tindle, A. G. 1984. Trace element discrimination diagrams for the tectonic interpretation of granitic rocks. *Journal of Petrology* 25, 956–983.
- Pupin, J. P. 1980. Zircon and granite petrology. *Contributions to Mineralogy and Petrology* 73, 207–220.
- Raup, D. M. & Sepkoski, J. J. 1982. Mass extinctions in the marine fossil record. *Science* 215, 1501–1503.
- Samson, S. D. & Alexander, E. C., Jr. 1987. Calibration of the interlaboratory $^{40}\text{Ar}/^{39}\text{Ar}$ dating standard, MMhb-1. *Chemical Geology* 66, 27–34.
- Satterthwaite, F. E. 1946. An approximate distribution of estimates of variance components. *Biometrics Bulletin* 2, 110–114.
- Shibata, K. 1992. Radiometric dating of the Late Cretaceous sequences in Hokkaido, Japan. *Abstracts of 29th International Geological Congress, Kyoto, Japan* 1, 88.
- Stacey, J. S. & Kramers, J. D. 1975. Approximation of terrestrial lead isotope evolution by a two-stage model. *Earth and Planetary Science Letters* 26, 207–221.
- Staudacher, Th., Jessberger, E. K., Dorflinger, D. & Kiko, J. 1978. A refined ultrahigh-vacuum furnace for rare gas analysis. *Journal of Physics E: Scientific Instruments* 11, 781–784.
- Steiger, R. H. & Jäger, E. 1977. Subcommittee on geochronology: convention on the use of decay constants in geo- and cosmo-chronology. *Earth and Planetary Science Letters* 36, 359–363.
- Taylor, J. R. 1982. An introduction to error analysis (University of Science Books, Mill Valley, California).
- Williams, G. D. & Baadsgaard, H. 1975. Potassium-argon dates and Upper Cretaceous biostratigraphy in eastern Saskatchewan. *Geological Association of Canada, Special Paper* 13, 417–426.
- Winchester, J. A. & Floyd, P. A. 1977. *Geochemical discrimination of different magma series and their differentiation products using immobile elements*. *Chemical Geology* 20, 325–343.
- Wintsch, R. P., Kunk, M. J., Cortesini, H. Jr & Sutter, J. F. 1991. $^{40}\text{Ar}/^{39}\text{Ar}$ age spectrum data for the Avalon and Putman-Nashoba lithotectonic zones, eastern Connecticut and western Rhode Island. *US Geological Survey Open File Report* 91-399, 133 pp.